

MIT Open Access Articles

Measurement of the CP-violating phase β in $B^0 \rightarrow [J/\psi] \pi^+ \pi^-$ decays and limits on penguin effects

The MIT Faculty has made this article openly available. **Please share** how this access benefits you. Your story matters.

Citation: "Measurement of the CP-Violating Phase β in $B^0 \rightarrow [J/\psi] \pi^+ \pi^-$ Decays and Limits on Penguin Effects." Physics Letters B 742 (March 2015): 38–49.

As Published: <http://dx.doi.org/10.1016/j.physletb.2015.01.008>

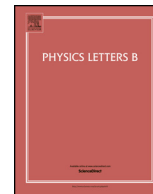
Publisher: Elsevier

Persistent URL: <http://hdl.handle.net/1721.1/94637>

Version: Final published version: final published article, as it appeared in a journal, conference proceedings, or other formally published context

Terms of use: Creative Commons Attribution





Measurement of the CP-violating phase β in $B^0 \rightarrow J/\psi \pi^+ \pi^-$ decays and limits on penguin effects



LHCb Collaboration

ARTICLE INFO

Article history:

Received 6 November 2014
 Received in revised form 23 December 2014
 Accepted 7 January 2015
 Available online 13 January 2015
 Editor: W.-D. Schlatter

ABSTRACT

Time-dependent CP violation is measured in the $\bar{B}^0 \rightarrow J/\psi \pi^+ \pi^-$ channel for each $\pi^+ \pi^-$ resonant final state using data collected with an integrated luminosity of 3.0 fb^{-1} in pp collisions using the LHCb detector. The final state with the largest rate, $J/\psi \rho^0(770)$, is used to measure the CP-violating angle $2\beta^{\text{eff}}$ to be $(41.7 \pm 9.6^{+2.8}_{-6.3})^\circ$. This result can be used to limit the size of penguin amplitude contributions to CP violation measurements in, for example, $\bar{B}_s^0 \rightarrow J/\psi \phi$ decays. Assuming approximate SU(3) flavour symmetry and neglecting higher order diagrams, the shift in the CP-violating phase ϕ_s is limited to be within the interval $[-1.05^\circ, +1.18^\circ]$ at 95% confidence level. Changes to the limit due to SU(3) symmetry breaking effects are also discussed.

© 2015 The Authors. Published by Elsevier B.V. This is an open access article under the CC BY license (<http://creativecommons.org/licenses/by/4.0/>). Funded by SCOAP³.

1. Introduction

Measurements of CP violation in neutral B meson decays are used either to search for physics beyond the Standard Model (SM) [1] or set limits on combinations of Cabibbo–Kobayashi–Maskawa couplings (V_{ij}) [2]. Interpretations of the measurement of the CP-violating phase 2β via the interference of mixing and decays in the $\bar{B}^0 \rightarrow J/\psi K_S^0$ channel, and the phase ϕ_s in $\bar{B}_s^0 \rightarrow J/\psi \phi$ and $J/\psi \pi^+ \pi^-$ decays,¹ are made assuming that the decays are dominated by tree-level processes. However, penguin processes are also possible, and they may have amplitudes large enough to influence the results. Here we use $\bar{B}^0 \rightarrow J/\psi \pi^+ \pi^-$ decays to set limits on possible changes due to penguin contributions. This mode has both tree and penguin diagrams, as shown in Fig. 1. Theoretical models, to be discussed later, predict that the ratio of penguin to tree amplitudes is greatly enhanced in this decay relative to $\bar{B}^0 \rightarrow J/\psi K_S^0$ [3,4]. Thus, the effects of penguin topologies can be investigated by using the $J/\psi \pi^+ \pi^-$ decay and comparing differ-

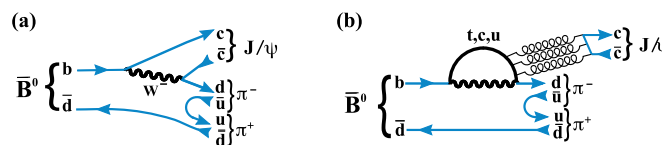


Fig. 1. (a) Tree level and (b) penguin diagram for \bar{B}^0 decays into $J/\psi \pi^+ \pi^-$.

ent measurements of the CP-violating phase 2β in $J/\psi K_S^0$, and individual channels such as $\bar{B}^0 \rightarrow J/\psi \rho^0(770)$.²

Next, we discuss the time-dependent decay rate, taking into account that the $\pi^+ \pi^-$ system is composed of the resonances previously reported in Ref. [5]. This analysis largely follows the measurement procedure used in the study of CP violation in \bar{B}_s^0 decays into $J/\psi \pi^+ \pi^-$ [6]. The total decay amplitude for \bar{B}^0 at a decay time of zero is taken to be the sum over individual $\pi^+ \pi^-$ resonant transversity amplitudes [7], and possibly one non-resonant amplitude, with each component labeled as A_i (\bar{A}_i). The quantities q and p relate the mass eigenstates to the flavor eigenstates [8]. By introducing the parameter $\lambda_i \equiv \frac{q}{p} \frac{\bar{A}_i}{A_i}$, relating CP violation in the interference between mixing and decay associated with the state i , the amplitudes \mathcal{A} and $\bar{\mathcal{A}}$ can be expressed as the sums of the individual \bar{B}^0 amplitudes, $\mathcal{A} = \sum A_i$ and $\bar{\mathcal{A}} = \sum \frac{q}{p} \frac{\bar{A}_i}{A_i} = \sum \lambda_i A_i =$

¹ CP violation measurements in $\bar{B}^0 \rightarrow J/\psi K_S^0$ determine the sum of $2\beta \equiv 2 \arg(-V_{cd}V_{cb}^*/(V_{td}V_{tb}^*))$ and contributions from higher order diagrams. Similar measurements in the \bar{B}_s^0 system determine ϕ_s which is the sum of $-2\beta_s \equiv -2 \arg(-V_{ts}V_{tb}^*/(V_{cs}V_{cb}^*))$ and higher order corrections.

² In the following ρ^0 or ρ refers to the $\rho^0(770)$ meson.

$\sum \eta_i |\lambda_i| e^{-i2\beta_i^{\text{eff}}} A_i$. For each transversity state i the CP -violating phase $2\beta_i^{\text{eff}} \equiv -\arg(\eta_i \lambda_i)$ with η_i being the CP eigenvalue of the state.³ The decay rates are⁴

$$\begin{aligned} \Gamma(t) &= \mathcal{N} e^{-\Gamma_d t} \left\{ \frac{|\mathcal{A}|^2 + |\bar{\mathcal{A}}|^2}{2} + \frac{|\mathcal{A}|^2 - |\bar{\mathcal{A}}|^2}{2} \cos(\Delta m_d t) \right. \\ &\quad \left. - \mathcal{I}m(A^* \bar{A}) \sin(\Delta m_d t) \right\}, \\ \bar{\Gamma}(t) &= \mathcal{N} e^{-\Gamma_d t} \left\{ \frac{|\mathcal{A}|^2 + |\bar{\mathcal{A}}|^2}{2} - \frac{|\mathcal{A}|^2 - |\bar{\mathcal{A}}|^2}{2} \cos(\Delta m_d t) \right. \\ &\quad \left. + \mathcal{I}m(A^* \bar{A}) \sin(\Delta m_d t) \right\}. \end{aligned} \quad (1)$$

2. Penguin and tree amplitudes

The decay $B^0 \rightarrow J/\psi K_S^0$ can be written as the sum of one tree level amplitude, similar to that shown in Fig. 1(a), but where the virtual W^- transforms to a $\bar{c}s$ pair, and three penguin amplitudes similar to those shown in Fig. 1(b). Here we neglect higher order diagrams. The t -quark mediated penguin amplitude can be expressed in terms of the other two using CKM unitarity. The resulting decay amplitude is [3]

$$A(B^0 \rightarrow J/\psi K_S^0) = \left(1 - \frac{\tilde{\lambda}^2}{2}\right) \mathcal{A} \left[1 + \frac{\tilde{\lambda}^2}{1 - \tilde{\lambda}^2} a e^{i\theta} e^{i\gamma}\right], \quad (2)$$

where $\tilde{\lambda} = |V_{us}| = 0.2252$ [10], $\gamma \equiv \arg(-V_{ud} V_{ub}^* / V_{cd} V_{cb}^*)$, \mathcal{A} denotes the sum of tree and penguin strong amplitudes, and a and θ are the magnitude and phase of the strong parts of the effective penguin amplitude relative to the tree amplitude.

For the case of $\bar{B}^0 \rightarrow J/\psi \pi^+ \pi^-$ decays, the $\pi^+ \pi^-$ pairs are in spin states ranging from zero to two. Since they are in a final state with a spin-1 J/ψ resonance, the amplitudes in the different transversity states f need to be distinguished for all spins above zero. For example, the amplitude for each $J/\psi \rho^0(770)$ transversity state is

$$-\sqrt{2} A(B^0 \rightarrow (J/\psi \rho)_f) = \tilde{\lambda} \mathcal{A}' [1 - a'_f e^{i\theta'_f} e^{i\gamma}], \quad (3)$$

where the primed quantities are defined in analogy with the unprimed ones in Eq. (2). For \bar{B}^0 decays only the sign in front of $i\gamma$ changes. We are only concerned here with the relative size of the tree and penguin amplitudes. For $J/\psi K_S^0$ the penguin is suppressed relative to the tree by an additional factor of $\epsilon \equiv \tilde{\lambda}^2 / (1 - \tilde{\lambda}^2) = 0.0534$. Thus, comparing even a relatively poor measurement of $2\beta^{\text{eff}}$ measured in $J/\psi \rho^0$ with 2β measured in $J/\psi K_S^0$ allows us to set stringent limits on the penguin contribution. Using approximate SU(3) flavor symmetry the size of the penguin contribution in $\bar{B}^0 \rightarrow J/\psi \rho^0$ can be related to that in $\bar{B}_s^0 \rightarrow J/\psi \phi$ decays as pointed out in Refs. [4,11].

We now turn to the expressions for CP violation in the presence of both tree and penguin amplitudes. The complex-valued CP parameter λ_f is given by

$$\lambda_f \equiv \frac{q}{p} \frac{A(\bar{B}^0 \rightarrow (J/\psi \rho)_f)}{A(B^0 \rightarrow (J/\psi \rho)_f)} = \eta_f \frac{1 - a'_f e^{i\theta'_f} e^{-i\gamma}}{1 - a'_f e^{i\theta'_f} e^{i\gamma}} e^{-2i\beta}, \quad (4)$$

where β is the phase induced by mixing. Thus the measured phase β_f^{eff} is related to β by

$$\eta_f \lambda_f \equiv |\lambda_f| e^{-i2\beta_f^{\text{eff}}} = \frac{1 - a'_f e^{i\theta'_f} e^{-i\gamma}}{1 - a'_f e^{i\theta'_f} e^{i\gamma}} e^{-i2\beta}, \quad (5)$$

separating real and imaginary parts gives

$$|\lambda_f| = \left| \frac{1 - a'_f e^{i\theta'_f} e^{-i\gamma}}{1 - a'_f e^{i\theta'_f} e^{i\gamma}} \right|, \quad \text{and}$$

$$\Delta 2\beta_f \equiv 2\beta_f^{\text{eff}} - 2\beta = -\arg\left(\frac{1 - a'_f e^{i\theta'_f} e^{-i\gamma}}{1 - a'_f e^{i\theta'_f} e^{i\gamma}}\right). \quad (6)$$

For the $J/\psi K_S^0$ mode we replace a'_f and θ'_f in Eq. (6) by $-\epsilon a_f$ and θ_f , respectively. In addition, we take $a' = a$ and $\theta' = \theta$. The relationship between the penguin influence on the mixing induced CP violation phase in favored decays and the measurements in $\bar{B}^0 \rightarrow (J/\psi \rho^0)_f$ is then given by

$$\delta_P = -\arg\left(\frac{(\lambda'_f e^{2i\gamma} - 1) + \epsilon(\lambda'_f - 1)}{(\lambda'_f e^{2i\gamma} - 1) + \epsilon(\lambda'_f - 1)e^{2i\gamma}}\right)$$

where $\lambda'_f \equiv |\lambda_f| e^{-i\Delta 2\beta_f}$. (7)

We will show that the penguin shift has a weak dependence on $|\lambda_f|$, resulting in $\delta_P \approx -\epsilon \Delta 2\beta_f$. Since the uncertainty on the current measurement of 2β is $(_{-1.5}^{+1.6})^\circ$, a measurement of $\Delta 2\beta_f$, even with an uncertainty ten times larger, could limit penguin contributions to be well below the current statistical uncertainty, which is the main aim of this analysis.

3. Detector software and event selection

The LHCb detector [12] is a single-arm forward spectrometer covering the pseudorapidity range $2 < \eta < 5$, designed for the study of particles containing b or c quarks. The detector includes a high-precision tracking system consisting of a silicon-strip vertex detector surrounding the pp interaction region [13], a large-area silicon-strip detector located upstream of a dipole magnet with a bending power of about 4 Tm, and three stations of silicon-strip detectors and straw drift tubes [14] placed downstream of the magnet. The tracking system provides a measurement of momentum,⁵ p , with a relative uncertainty that varies from 0.4% at low momentum to 0.6% at 100 GeV. The minimum distance of a track to a primary vertex (PV), the impact parameter (IP), is measured with a resolution of $(15 + 29/p_T) \mu\text{m}$, where p_T is the component of p transverse to the beam, in GeV. Different types of charged hadrons are distinguished using information from two ring-imaging Cherenkov detectors [15]. Photon, electron and hadron candidates are identified by a calorimeter system consisting of scintillating-pad and preshower detectors, an electromagnetic calorimeter and a hadronic calorimeter. Muons are identified by a system composed of alternating layers of iron and multiwire proportional chambers [16].

The trigger [17] consists of a hardware stage, based on information from the calorimeter and muon systems, followed by a software stage that applies a full event reconstruction [17]. Events selected for this analysis are triggered by a $J/\psi \rightarrow \mu^+ \mu^-$ decay, where the J/ψ meson is required at the software level to be consistent with coming from the decay of a \bar{B}^0 meson by use of either of IP requirements or detachment of the J/ψ meson decay vertex

³ Note that while q/p and \bar{A}_i/A_i are phase convention dependent, λ_i is not.

⁴ We assume $\Delta\Gamma_d = 0$ and $|p/q| = 1$. The averages of current measurements are $\Delta\Gamma_d/\Gamma_d = 0.001 \pm 0.010$ and $|p/q| = 1.0005 \pm 0.0011$ [9].

⁵ We use natural units where $\hbar = c = 1$.

from the primary vertex. In the simulation, pp collisions are generated using PYTHIA [18] with a specific LHCb configuration [19]. Decays of hadronic particles are described by EVTGEN [20], in which final state radiation is generated using PHOTOS [21]. The interaction of the generated particles with the detector and its response are implemented using the GEANT4 toolkit [22] as described in Ref. [23].

A $\bar{B}^0 \rightarrow J/\psi\pi^+\pi^-$ candidate is reconstructed by combining a $J/\psi \rightarrow \mu^+\mu^-$ candidate with two pions of opposite charge. The like-sign combinations $J/\psi\pi^\pm\pi^\pm$ are also reconstructed for background studies. The event selection is described in detail in the time-integrated amplitude analysis [5]. The only difference here is that we reject $K_S^0 \rightarrow \pi^+\pi^-$ candidates by excluding the events in the region within ± 20 MeV of the K_S^0 mass peak.

Only candidates with dimuon invariant mass between -48 MeV and $+43$ MeV relative to the observed J/ψ mass peak are selected, corresponding a window of about $\pm 3\sigma$. The two muons subsequently are kinematically constrained to the known J/ψ mass. Other requirements are imposed to isolate \bar{B}^0 candidates with high signal yield and minimum background. This is accomplished by combining the $J/\psi \rightarrow \mu^+\mu^-$ candidate with a pair of pion candidates of opposite charge, and then testing if all four tracks form a common decay vertex. Pion candidates are each required to have p_T greater than 250 MeV, and the scalar sum of the two transverse momenta, $p_T(\pi^+) + p_T(\pi^-)$, must be larger than 900 MeV. To test for inconsistency with production at the PV, the IP χ^2 is computed as the difference between the χ^2 of the PV reconstructed with and without the considered track. Each pion must have an IP χ^2 greater than 9. Pion and kaon candidates are positively identified using the RICH system. The four-track \bar{B}^0 candidate must have a flight distance of more than 1.5 mm, where the average decay length resolution is 0.17 mm. The angle between the combined momentum vector of the decay products and the vector formed from the positions of the PV and the decay vertex (pointing angle) is required to be less than 2.5° . Events satisfying this preselection are then further filtered using a multivariate analyzer based on a Boosted Decision Tree (BDT) technique [24]. The BDT uses eight variables that are chosen to provide separation between signal and background. These are the minimum of $\text{DLL}(\mu - \pi)$ of the μ^+ and μ^- , $p_T(\pi^+) + p_T(\pi^-)$, the minimum of IP χ^2 of the π^+ and π^- , and the \bar{B}^0 properties of vertex χ^2 , pointing angle, flight distance, p_T and IP χ^2 , where $\text{DLL}(\mu - \pi)$ is a logarithm of the likelihood ratio between μ and π hypotheses for the muon candidates.

The BDT is trained on a simulated sample of two million $\bar{B}^0 \rightarrow J/\psi\pi^+\pi^-$ signal events generated uniformly in phase space with unpolarized $J/\psi \rightarrow \mu^+\mu^-$ decays, and a background data sample from the sideband $5566 < m(J/\psi\pi^+\pi^-) < 5616$ MeV. Then separate samples are used to train and test the BDT.

The invariant mass of the selected $J/\psi\pi^+\pi^-$ combinations, where the dimuon pair is constrained to have the J/ψ mass, is shown in Fig. 2. There is a large peak at the \bar{B}_s^0 mass and a smaller one at the \bar{B}^0 mass on top of the background. A double Crystal Ball function with common means models the radiative tails and is used to fit each of the signals [25]. Other components in the fit model take into account background contributions from $B^- \rightarrow J/\psi K^-$ and $B^- \rightarrow J/\psi\pi^-$ decays combined with a random π^+ , $\bar{B}_s^0 \rightarrow J/\psi\eta(\prime)$ with $\eta(\prime) \rightarrow \pi^+\pi^-\gamma$, $\bar{B}_s^0 \rightarrow J/\psi\phi$ with $\phi \rightarrow \pi^+\pi^-\pi^0$, $\bar{B}^0 \rightarrow J/\psi K^-\pi^+$ and $\Lambda_b^0 \rightarrow J/\psi K^-p$ reflections, and combinatorial backgrounds. The exponential combinatorial background shape is taken from like-sign combinations, that are the sum of $\pi^+\pi^+$ and $\pi^-\pi^-$ candidates. The shapes of the other components are taken from the simulation with their normalizations allowed to vary. Only the candidates within ± 20 MeV of the B^0 mass peak are retained for CP violation measurements;

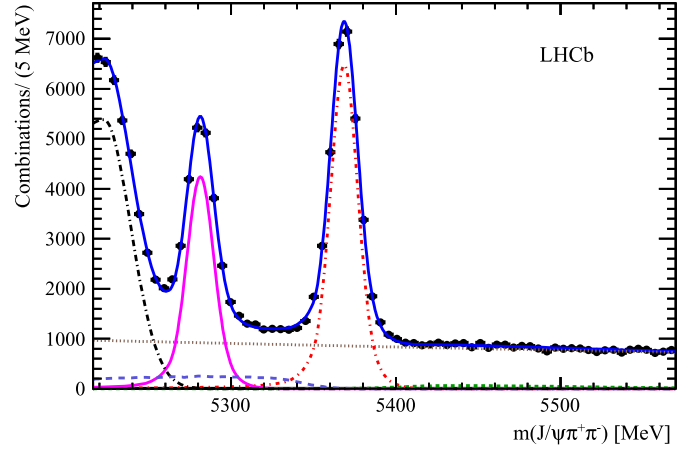


Fig. 2. Invariant mass of $J/\psi\pi^+\pi^-$ combinations with K_S^0 veto. The data have been fitted with double-Crystal ball signal and several background functions. The (purple) solid line shows the \bar{B}^0 signal, the (brown) dotted line shows the combinatorial background, the (green) short-dashed shows the B^- background, the (red) dot-dashed is $\bar{B}_s^0 \rightarrow J/\psi\pi^+\pi^-$, the (light blue) long-dashed is the sum of $\bar{B}_s^0 \rightarrow J/\psi\eta'$, $\bar{B}_s^0 \rightarrow J/\psi\phi$ when $\phi \rightarrow \pi^+\pi^-\pi^0$ backgrounds and the $\Lambda_b^0 \rightarrow J/\psi K^-p$ reflection, the (black) dot-long dashed is the $\bar{B}^0 \rightarrow J/\psi K^-\pi^+$ reflection and the (blue) solid line is the total. (For interpretation of the references to color in this figure legend, the reader is referred to the web version of this article.)

the fit gives 17650 ± 200 signal and 9840 ± 160 background candidates.

4. The signal likelihood

We fit the entire $\pi^+\pi^-$ mass spectrum, by including the resonance contributions found in the amplitude analysis [5], in order to measure the CP -violating parameters of all the states, the most important being $\bar{B}^0 \rightarrow J/\psi\rho^0$ as it has the largest fit fraction of approximately 65%. The same likelihood construction as was used to determine the CP -violating quantities ϕ_s and $|\lambda|$ in $\bar{B}_s^0 \rightarrow J/\psi\pi^+\pi^-$ decays [6] is employed. Here the value of $\Delta\Gamma_d \approx 0$ simplifies some terms, and the smaller value of Δm_d makes the decay time resolution function less important. In addition, a different same-sign flavor tagging algorithm is used.

The determination of the CP violation parameters relies upon the formalism developed in Ref. [26]. For J/ψ decays to $\mu^+\mu^-$ final states the amplitudes are themselves functions of four variables: the $\pi^+\pi^-$ invariant mass $m_{hh} = m(\pi^+\pi^-)$, and three angles Ω , defined in the helicity basis. These consist of: $\theta_{J/\psi}$, the angle between the μ^+ direction in the J/ψ rest frame with respect to the J/ψ direction in the \bar{B}^0 rest frame; θ_{hh} , the angle between the h^+ direction in the h^+h^- rest frame with respect to the h^+h^- direction in the \bar{B}^0 rest frame; and χ , the angle between the J/ψ and h^+h^- decay planes in the \bar{B}^0 rest frame [26,27].

We perform a simultaneous unbinned maximum likelihood fit to the decay time t , m_{hh} , and the three helicity angles Ω , along with information on the initial flavor of the decaying hadron, *i.e.* whether it was produced as a B^0 or a \bar{B}^0 meson. The probability density function (PDF) used in the fit consists of signal and background components that include detector resolution and acceptance effects. The predicted decay time error for each event is used for the decay time resolution model, and similarly the measured per-event misidentification probability is used for determining the initial flavor of the neutral B meson. The $\pi^+\pi^-$ invariant mass distribution is shown in Fig. 3 along with the fitted components of the different resonances using the ‘‘Best model’’ [5] for the $\pi^+\pi^-$ resonance content.

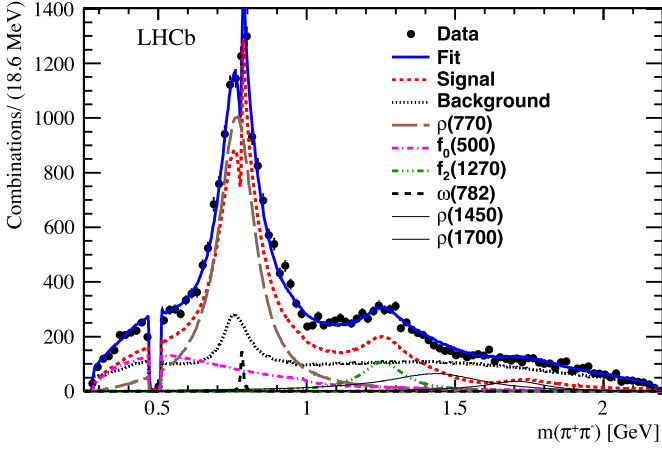


Fig. 3. Fit projection of $m(\pi^+\pi^-)$ showing the different resonant contributions in the “Best model” [5]. The K_S^0 veto causes the absence of events near 500 MeV. The shape variation near 780 MeV is due to interference between the $\rho(770)$ and $\omega(782)$ states. The total fit is the sum of the individual components plus their interferences.

Knowledge of the \bar{B}^0 flavor at production, called “tagging”, is necessary to measure CP violation. We use both opposite-side (OS) [28] and same-side pion ($SS\pi$) tagging information; here we use the same procedure as for same-side kaon tagging used in the $\bar{B}_s^0 \rightarrow J/\psi\pi^+\pi^-$ and $J/\psi\phi$ analyses [27], but identify the tag from a pion rather than a kaon. The wrong-tag probability η is estimated based on the output of a neural network trained on simulated data. It is calibrated with data using flavor-specific decay modes in order to predict the true wrong-tag probability of the event $\bar{B}^0(\eta)$ for an initial flavor \bar{B}^0 meson, which has a linear dependence on η . The calibration is performed separately for the OS and the $SS\pi$ taggers. If events are tagged by both OS and $SS\pi$ algorithms, a combined tag decision and wrong-tag probability are given by the algorithm defined in Ref. [28]. This combined algorithm is implemented in the overall fit. The effective tagging power obtained is characterized by $\varepsilon_{\text{tag}} D^2 = (3.26 \pm 0.17)\%$, where $D \equiv (1 - 2\omega_{\text{avg}})$ is the dilution, ω_{avg} is the average wrong-tag probability for ω and $\bar{\omega}$, and $\varepsilon_{\text{tag}} = (42.1 \pm 0.6)\%$ is the signal tagging efficiency.

The signal decay time distribution including flavor tagging is

$$R(\hat{t}, m_{hh}, \Omega, q|\eta) = \frac{1}{1 + |q|} \left[[1 + q(1 - 2\omega(\eta))] \Gamma(\hat{t}, m_{hh}, \Omega) + [1 - q(1 - 2\bar{\omega}(\eta))] \frac{1 + A_P}{1 - A_P} \bar{\Gamma}(\hat{t}, m_{hh}, \Omega) \right], \quad (8)$$

where \hat{t} is the true decay time, $\bar{\Gamma}$ is defined in Eq. (1), and $A_P = -0.0035 \pm 0.0081$ [29] is the \bar{B}^0 - B^0 production asymmetry in the LHCb acceptance. The flavor tag parameter q takes values of -1 or $+1$ if the signal meson is tagged as \bar{B}^0 , B^0 respectively, or 0 if untagged.

The signal function is convolved with the decay time resolution and multiplied by the acceptance:

$$F^{\text{sig}}(t, m_{hh}, \Omega, q|\eta, \delta_t) = [R(\hat{t}, m_{hh}, \Omega, q|\eta) \otimes T(t - \hat{t}; \delta_t)] \cdot \mathcal{E}_t(t) \cdot \varepsilon(m_{hh}, \Omega), \quad (9)$$

where $\varepsilon(m_{hh}, \Omega)$ is the efficiency as a function of the h^+h^- mass and angles, obtained from the simulation as described in Ref. [5], $T(t - \hat{t}; \delta_t)$ is the decay time resolution function which depends upon the estimated decay time error for each event δ_t , and $\mathcal{E}_t(t)$

is the decay time acceptance function. The decay time resolution function $T(t - \hat{t}; \delta_t)$ is described by a sum of three Gaussian functions with a common mean. Studies using simulated data show that $J/\psi\pi^+\pi^-$ combinations produced directly in the pp interaction (prompt) have nearly identical resolution to signal events. Specifically, the time resolution is determined using prompt J/ψ decays into a dimuon pair, using a dedicated trigger for calibration purposes, plus two oppositely charged tracks from the primary vertex with the similar selection criteria as for $J/\psi\pi^+\pi^-$ and an invariant mass within ± 20 MeV of the B^0 mass. The effective resolution is found to be about 40 fs by using the weighted average widths of the three Gaussians. This is negligibly small compared to the \bar{B}^0 - B^0 oscillation time.

The decay time distribution is influenced by acceptance effects that are introduced by track reconstruction, trigger and event selection. The decay time acceptance is obtained using control samples of $\bar{B}^0 \rightarrow J/\psi K^{*0} (\rightarrow K^\mp \pi^\pm)$ decays, corrected by the acceptance ratio between $J/\psi K^\mp \pi^\pm$ and $J/\psi \pi^+\pi^-$ derived from simulation.

The acceptance function for the control sample is defined as

$$A(t; a, n, t_0, \beta_1, \beta_2) = \frac{[a(t - t_0)]^n}{1 + [a(t - t_0)]^n} \times (1 + \beta_1 t + \beta_2 t^2), \quad (10)$$

where $a, n, t_0, \beta_1, \beta_2$ are parameters determined by the fit. The decay time distribution of $\bar{B}^0 \rightarrow J/\psi K^\mp \pi^\pm$ candidates is described by the function

$$P^0(t) = \left(f_0 A(t; a, n, t_0, \beta_1, \beta_2) \frac{e^{-t/\tau_{B^0}}}{\tau_{B^0} \mathcal{N}_{B^0}^0} + (1 - f_0) A(t; a_{\text{bkg}}^0, n_{\text{bkg}}^0, 0, 0, 0) \frac{e^{-t/\tau_{\text{bkg}}^0}}{\tau_{\text{bkg}}^0 \mathcal{N}_{\text{bkg}}^0} \right) \otimes T(t - \hat{t}; \delta_t), \quad (11)$$

where f_0 is the signal fraction, and \mathcal{N}_{B^0} and $\mathcal{N}_{\text{bkg}}^0$ are normalizations necessary to construct PDFs of signal and background, respectively. The background acceptance function in Eq. (11) uses the same form as the signal and its parameters $a_{\text{bkg}}^0, n_{\text{bkg}}^0$ and τ_{bkg}^0 are obtained from mass sideband regions of 5180–5205 MeV and 5400–5425 MeV. The lifetime is constrained to $\tau_{B^0} = 1.519 \pm 0.007$ ps [10].

We use the product of the acceptance $A(a, n, t_0, \beta_1, \beta_2)$ determined from $\bar{B}^0 \rightarrow J/\psi K^{*0}$ and the correction ratio found from simulation as the time acceptance function for $\bar{B}^0 \rightarrow J/\psi\pi^+\pi^-$ events,

$$\mathcal{E}_t(t; a, n, t_0, \beta_1, \beta_2, p_1, p_2) = \frac{[a(t - t_0)]^n}{1 + [a(t - t_0)]^n} \times (1 + \beta_1 t + \beta_2 t^2) \times (1 - p_2 e^{-p_1 t}), \quad (12)$$

with parameter values and correlations given in Table 1.

5. Measurements of $2\beta^{\text{eff}}$

The CP -violating parameters are determined from a fit that uses the amplitude model with six final state $\pi^+\pi^-$ resonances. In our previous amplitude analysis [5] we used two parameterizations of the $f_0(500)$ resonance, “default” and “alternate”. The default used a Breit–Wigner resonance shape, with relatively poorly measured parameters, while the alternate used a function suggested by Bugg [30], with more theoretically motivated shape parameters. In this analysis we choose to switch to the shape suggested by Bugg, while the Breit–Wigner shape of the previous default parameterization is used to assess systematic uncertainties. A Gaussian

Table 1
Parameter values and correlations for the acceptance function $\varepsilon_t(t)$ in Eq. (12).

P	n	a	β_1	β_2	t_0	p_1	p_2	Values
n	1.000	0.444	0.574	-0.536	-0.862	0.000	0.000	2.082 ± 0.036
a		1.000	0.739	-0.735	-0.050	0.000	0.000	$1.981 \pm 0.024 \text{ ps}^{-1}$
β_1			1.000	-0.899	-0.374	0.000	0.000	$0.077 \pm 0.009 \text{ ps}^{-1}$
β_2				1.000	0.343	0.000	0.000	$-0.008 \pm 0.001 \text{ ps}^{-2}$
t_0					1.000	0.000	0.000	$0.104 \pm 0.003 \text{ ps}$
p_1						1.000	-0.885	$6.237 \pm 1.669 \text{ ps}^{-1}$
p_2							1.000	-0.739 ± 0.424

Table 2
Fit results for $2\beta_i^{\text{eff}}$ and α_{CP}^i .

Condition	$2\beta_i^{\text{eff}}$ ($^\circ$)	$\alpha_{CP}^i (\times 10^{-3})$
Fit 1	ρ	$41.7 \pm 9.6^{+2.8}_{-6.3}$
	other - ρ	$3.6 \pm 3.6^{+0.9}_{-0.8}$
Fit 2	ρ_0	$44.1 \pm 10.2^{+3.0}_{-6.9}$
	$\rho_{\parallel} - \rho_0$	$-0.8 \pm 6.5^{+1.9}_{-1.3}$
	$\rho_{\perp} - \rho_0$	$-3.6 \pm 7.2^{+2.0}_{-1.4}$
	other - ρ_0	$2.7 \pm 3.9^{+1.0}_{-0.9}$

constraint using $\Delta m_d = 0.510 \pm 0.003 \text{ ps}^{-1}$ [10] is applied in the fit. All other parameters, such as the time resolution, and those describing the tagging are fixed. In addition to the CP -violating parameters, the other free parameters are the amplitudes and phases of the resonances. To minimize correlations in the fitted results, we choose as free parameters the CP asymmetry $\alpha_{CP}^i = \frac{1-|\lambda_i|}{1+|\lambda_i|}$, $2\beta_i^{\text{eff}}$ of the largest polarization component, and $\Delta 2\beta_i^{\text{eff}}$ of the other components with respect to the largest one.

As $J/\psi\rho$ is the final state with the largest contribution, we treat it specially and perform two fits. In both cases all resonances other than the ρ share a common CP violation parameter λ' . For Fit 1 the three ρ transversity states share the same CP violation parameter λ , while for Fit 2 each ρ transversity state has its own CP violation parameter λ_i . The results are shown in Table 2. The statistical uncertainties are within $\pm 15\%$ of the precision estimated using toy Monte Carlo simulation. To determine $\Delta 2\beta_f$ we use the measured value in $b \rightarrow c\bar{c}s$ transitions of $(42.8^{+1.6}_{-1.5})^\circ$ found in B^0 decays [9]. Our measurement of $2\beta^{\text{eff}}$ is consistent with this value for both Fit 1 and Fit 2. The correlation between α_{CP}^{ρ} and $2\beta_{\rho}^{\text{eff}}$ is -0.01 in Fit 1. Table 3 shows the correlation matrix for the CP -violating parameters in Fit 2.

Table 4 lists the fit fractions and three transversity fractions of contributing resonances from Fit 1, consistent with the results shown in the amplitude analysis [5]. For a P - or D -wave resonance, we report its total fit fraction by summing all three transversity components. This time-dependent analysis determines the phase difference between the CP -odd component of $\rho(770)_{\perp}$ and the CP -even component of $\rho(770)_0$ to be $(167 \pm 11)^\circ$ in Fit 1.

Table 3
The correlation matrix for the CP -violating parameters determined using Fit 2, where $\Delta 2\beta_i^{\text{eff}} = 2\beta_i^{\text{eff}} - 2\beta_{\rho_0}^{\text{eff}}$.

	$\alpha_{CP}^{\text{other}}$	$\alpha_{CP}^{\rho_0}$	$\alpha_{CP}^{\rho_{\perp}}$	$\alpha_{CP}^{\rho_{\parallel}}$	$\Delta 2\beta_{\text{other}}^{\text{eff}}$	$\Delta 2\beta_{\rho_{\perp}}^{\text{eff}}$	$\Delta 2\beta_{\rho_{\parallel}}^{\text{eff}}$	$2\beta_{\rho_0}^{\text{eff}}$
$\alpha_{CP}^{\text{other}}$	1.00	-0.62	-0.28	-0.13	0.05	-0.42	-0.19	0.05
$\alpha_{CP}^{\rho_0}$		1.00	0.03	0.16	0.29	0.22	0.16	-0.11
$\alpha_{CP}^{\rho_{\perp}}$			1.00	-0.21	-0.19	0.59	-0.07	0.10
$\alpha_{CP}^{\rho_{\parallel}}$				1.00	0.01	-0.04	-0.25	-0.09
$\Delta 2\beta_{\text{other}}^{\text{eff}}$					1.00	0.00	0.26	-0.16
$\Delta 2\beta_{\rho_{\perp}}^{\text{eff}}$						1.00	0.39	-0.08
$\Delta 2\beta_{\rho_{\parallel}}^{\text{eff}}$							1.00	-0.10
$2\beta_{\rho_0}^{\text{eff}}$								1.00

Table 4
Fit and transversity fractions of contributing resonances from Fit 1. Uncertainties are statistical only. These results are presented only as a cross-check.

Component	Fit fraction (%)	Transversity fractions (%)		
		0	\parallel	\perp
$\rho(770)$	65.6 ± 1.9	56.7 ± 1.8	23.5 ± 1.5	19.8 ± 1.7
$f_0(500)$	20.1 ± 0.7	1	0	0
$f_2(1270)$	7.8 ± 0.6	64 ± 4	9 ± 5	27 ± 5
$\omega(782)$	$0.64^{+0.19}_{-0.13}$	44 ± 14	53 ± 14	3_{-3}^{+10}
$\rho(1450)$	9.0 ± 1.8	47 ± 11	39 ± 12	14 ± 8
$\rho(1700)$	3.1 ± 0.7	29 ± 12	42 ± 15	29 ± 15

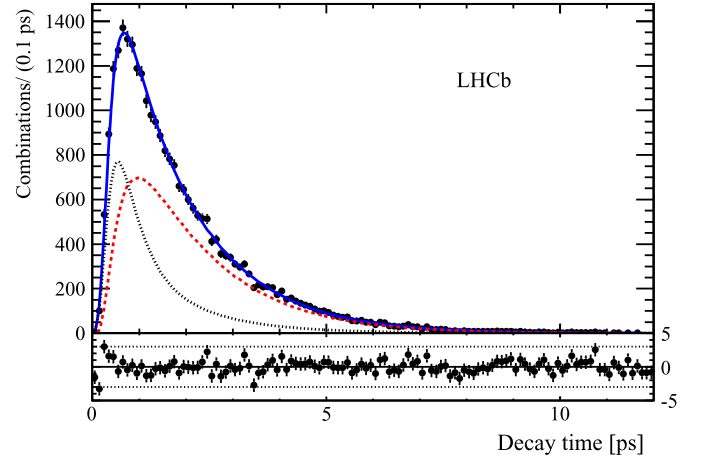


Fig. 4. Decay time distribution of $B^0 \rightarrow J/\psi\pi^+\pi^-$ candidates. The signal component is shown with a (red) dashed line, the background with a (black) dotted line, and the (blue) solid line represents the total. The lower plot shows the normalized residual distribution. (For interpretation of the references to color in this figure legend, the reader is referred to the web version of this article.)

This quantity is not accessible in the time-integrated amplitude analysis. Fig. 4 shows the decay time distribution superimposed with the fit projection.

The statistical significances of the CP measurements are ascertained by fitting the data requiring that CP -violating components

Table 5

Results allowing for different CP-violating effects for resonances other than the ρ in an extension of Fit 1.

$2\beta_i^{\text{eff}} (^\circ)$		$\alpha_{CP}^i (\times 10^{-3})$	
ρ	41.8 ± 9.6	ρ	2 ± 39
$f_0(500) - \rho$	2.7 ± 3.8	$f_0(500)$	-58 ± 46
$f_2(1270) - \rho$	1.8 ± 7.5	$f_2(1270)$	9 ± 63
other spin-1 $-\rho$	3.7 ± 11.1	other spin-1	15 ± 58

are zero. We find that for the entire final state, this requirement changes -2 times the logarithm of the likelihood ($-2 \ln \mathcal{L}$) by 28.6, corresponding to 4.4 standard deviations for four degrees of freedom (ndf), and for the $\rho(770)$ component only, the change is 24.0, corresponding to 4.5 standard deviations for two ndf. Here we only consider the statistical uncertainties.

We also perform a fit by extending Fit 1 to allow different CP-violating effects in final states with either the $f_0(500)$, the $f_2(1270)$, or spin-1 resonances. The results are shown in Table 5. We find that these fits all give consistent values of the CP-violating parameters.

The systematic uncertainties evaluated for both fit configurations are summarized for the CP-violating phases in Table 6 and for the magnitudes of the asymmetries in Table 7. They are small compared to the statistical ones. The two largest contributions result from the resonance fit model and the resonance parameters. Fit model uncertainties are determined by adding an additional resonance to the default six-resonance model, either the $f_0(980)$, the $f_0(1500)$, the $f_0(1700)$, or non-resonant $\pi^+\pi^-$, replacing the $f_0(500)$ model by a Breit-Wigner function, and using the alternative Gounaris-Sakurai model shapes [31] for the various ρ mesons. The largest variation among those changes is assigned as the systematic uncertainty for modeling. Including a non-resonant component gives the largest negative change on $2\beta^{\text{eff}}$ for the ρ and ρ^0 categories.

To evaluate the uncertainties due to the fixed parameters of resonances, we repeat the amplitude fit by varying the mass and width of all the resonances used in the six-resonance model within their errors one at a time, and add the changes in quadrature. To evaluate the systematic uncertainties due to the other fixed parameters including those in the decay time acceptance, the background decay time PDF, the $m(\pi^+\pi^-)$ distribution, the angular acceptance, and background mass PDF, the data fit is repeated by varying the fixed parameters from their nominal values according to the error matrix, one hundred times for each source. The matrix elements are determined using simulation, $B^0 \rightarrow J/\psi K^{*0}$ data, and like-sign $J/\psi\pi^\pm\pi^\pm$ data. The r.m.s. of the fitted physics parameter of interest is taken as its uncertainty for each source.

The acceptance model for each of the three angles as a function of m_{hh} is determined independently. To evaluate the reliability of this method we parameterize the mass and angle efficiencies as a combination of Legendre polynomials and spherical harmonics that takes into account all correlations. The amplitude fit is repeated using the new acceptance parameterizations; changes are found to be small and taken as the systematic uncertainty.

In the nominal fit the background is divided into three sources: background to the ρ^0 component from $B_s^0 \rightarrow J/\psi\eta', \eta' \rightarrow \rho^0\gamma$, reflection from $B^0 \rightarrow J/\psi K^{*0}$ when the kaon is misidentified as a pion, and the remaining background. The latter includes the reflections from $\Lambda_b^0 \rightarrow J/\psi K^\pm p$ decays, where both the kaon and proton are misidentified, and combinatorial background. The dependence on m_{hh} of the decay time distribution for this remaining background is modeled by using different decay time PDFs in different m_{hh} regions. We also change the background modeling

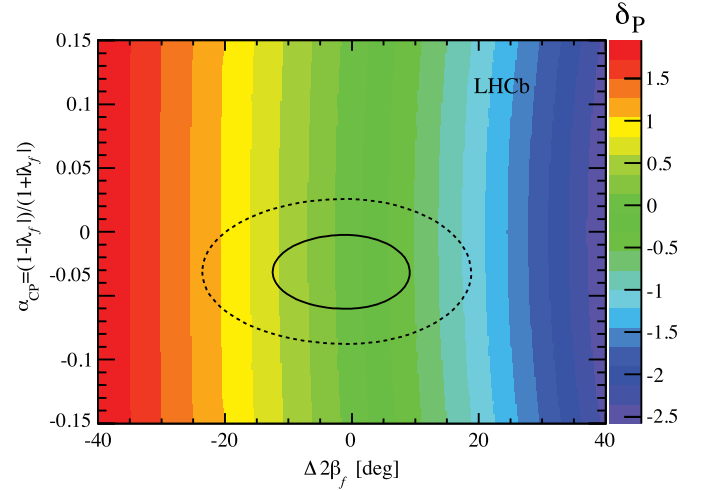


Fig. 5. The magnitude of the penguin induced shift δ_p on the CP-violating phase in favored decays, assuming SU(3) flavor symmetry, shown in grey or color scale in degrees, as a function of the measured difference $\Delta 2\beta_f$ (x-axis) and $\alpha_{CP} = \frac{1-\beta_f}{1+\beta_f}$ (y-axis). Here we use fixed values for $\gamma = 70^\circ$ and $\epsilon = 0.0534$. The projected 68% (solid) and 95% (dashed) confidence levels on δ_p are shown by the egg-shaped contours.

by dividing the remaining background into separate combinatorial and Λ_b^0 reflection components. The fit is repeated with the new background model, and changes are taken as the systematic uncertainty.

The systematic uncertainty due to the tagging parameter calibration is given by the difference in quadrature of the statistical uncertainties for each physics parameter between the nominal fit and an alternative fit where the tagging parameters are Gaussian constrained by their total uncertainties. The systematic uncertainty due to the asymmetry of $\bar{B}^0 - B^0$ meson production is estimated by varying the central value $A_p = -0.0035 \pm 0.0081$ [29] by its uncertainty.

6. Discussion of results and conclusions

We compare the ρ -only Fit 1 result of $2\beta^{J/\psi\rho} = 2\beta^{\text{eff}} = (41.7 \pm 9.6_{-6.3}^{+2.8})^\circ$ with the Cabibbo-favored B to charmonium result, denoted $J/\psi K_S^0$. The measured difference is

$$\Delta 2\beta_f = 2\beta^{J/\psi\rho} - 2\beta^{J/\psi K_S^0} = (-0.9 \pm 9.7_{-6.3}^{+2.8})^\circ. \quad (13)$$

Since the result is consistent with zero we determine limits on the magnitude of the CP-violating phase shift due to a possible penguin component in $b \rightarrow c\bar{c}s$ decays, δ_p . The limit is evaluated using pseudo-experiments by generating datasets with different values of α_{CP} , $2\beta^{J/\psi\rho} - 2\beta^{J/\psi K_S^0}$, and $\gamma = (70.0_{-9.0}^{+7.7})^\circ$ [9] according to the measured uncertainties, including the correlation of -0.01 between α_{CP} and $2\beta^{J/\psi\rho}$. Then δ_p for each dataset is calculated using Eq. (7). We find a Gaussian distribution with a 95% confidence level (CL) interval of $[-1.05^\circ, 1.18^\circ]$. This result is consistent with that obtained by projecting a contour of α_{CP} and $2\beta^{J/\psi\rho} - 2\beta^{J/\psi K_S^0}$ with regions proportional to the total uncertainties of the two physics variables as shown in Fig. 5.

The two reactions $B^0 \rightarrow J/\psi\rho^0$ and $B_s^0 \rightarrow J/\psi\phi$ are related by SU(3) symmetry if we also assume that the difference between the ϕ being mostly a singlet state, and the ρ^0 an octet state causes negligible breaking. Taking the magnitudes of the penguin amplitudes $a = a'$ and the strong phases $\theta = \theta'$ to be equal in $B^0 \rightarrow J/\psi\rho^0$ and $B_s^0 \rightarrow J/\psi\phi$ decays, and neglecting higher order diagrams [3], we find $\delta_p = (0.05 \pm 0.56)^\circ = 0.9 \pm 9.8$ mrad. At

Table 6
Systematic uncertainties on CP -violating phases $2\beta_i^{\text{eff}}$ ($^\circ$). Statistical uncertainties are also shown.

Fit Sources	Fit 1			Fit 2		
	ρ	other $-\rho$	ρ_0	$\rho_{\parallel} - \rho_0$	$\rho_{\perp} - \rho_0$	other $-\rho_0$
Resonance model	+1.85	+0.51	+1.99	+1.35	+1.50	+0.68
Resonance parameters	-5.94	-0.33	-6.56	-0.05	-0.59	-0.52
Mass and angular acceptance	± 1.21	± 0.43	± 1.35	± 0.68	± 0.57	± 0.60
Angular acc. correlation	± 0.27	± 0.05	± 0.28	± 0.21	± 0.16	± 0.05
Decay time acceptance	± 0.22	± 0.03	± 0.22	± 0.21	± 0.08	± 0.03
Decay time acceptance	± 0.05	± 0.02	± 0.06	± 0.04	± 0.04	± 0.03
Bkg. mass and angular PDF	± 0.43	± 0.09	± 0.47	± 0.22	± 0.26	± 0.11
Bkg. decay time PDF	± 0.14	± 0.05	± 0.12	± 0.06	± 0.08	± 0.07
Bkg. model	± 0.49	± 0.23	± 0.15	± 0.97	± 0.38	± 0.13
Flavor Tagging	± 1.46	± 0.03	± 1.66	± 0.44	± 0.86	± 0.01
Production asymmetry	± 0.17	± 0.50	± 0.28	± 0.09	± 0.49	± 0.42
Total systematic uncertainty	+2.8	+0.9	+3.0	+1.9	+2.0	+1.0
	-6.3	-0.8	-6.9	-1.3	-1.4	-0.9
Statistical uncertainty	± 9.6	± 3.6	± 10.2	± 6.5	± 7.2	± 3.9

Table 7
Systematic uncertainties for the magnitude of the asymmetries α_{CP}^i ($\times 10^{-3}$). Statistical uncertainties are also shown.

Fit Sources	Fit 1			Fit 2		
	ρ	other $-\rho$	ρ_0	ρ_{\parallel}	ρ_{\perp}	other $-\rho_0$
Resonance model	+6.0	+0.0	+3.7	+5.0	+16.4	+0.4
Resonance parameters	-0.0	-11.4	-0.0	-2.7	-0.0	-11.0
Mass and angular acceptance	± 5.2	± 6.1	± 7.8	± 3.1	± 9.2	± 7.3
Angular acc. correlation	± 0.6	± 0.5	± 0.8	± 0.8	± 1.6	± 0.7
Decay time acceptance	± 0.2	± 0.9	± 0.2	± 0.9	± 0.6	± 0.9
Decay time acceptance	± 0.1	± 0.1	± 0.2	± 0.3	± 1.1	± 0.1
Bkg. mass and angular PDF	± 0.9	± 1.5	± 0.8	± 2.5	± 4.6	± 1.2
Bkg. decay time PDF	± 0.5	± 0.4	± 0.6	± 0.5	± 1.7	± 0.4
Bkg. model	± 2.6	± 2.9	± 5.2	± 3.5	± 0.9	± 4.6
Flavor Tagging	± 2.8	± 2.5	± 0.5	± 1.0	± 10.7	± 1.6
Production asymmetry	± 3.0	± 0.5	± 2.5	± 1.1	± 0.4	± 0.3
Total systematic uncertainty	+9	+7	+11	+8	+22	+9
	-7	-14	-10	-6	-15	-14
Statistical uncertainty	± 28	± 25	± 34	± 60	± 109	± 27

95% CL, the penguin contribution in $B_S^0 \rightarrow J/\psi\phi$ decay is within the interval from -1.05° to $+1.18^\circ$. Relaxing these assumptions changes the limits on the possible penguin induced shift. Fig. 6 shows how δ_P varies as a function of $\theta - \theta'$, indicating that the 95% CL limit on penguin pollution can increase to at most $\pm 1.2^\circ$. The variation in δ_P is proportional to a/a' . Thus, when changing a/a' over the interval 0.5 to 1.5, the limit on the penguin shift at 95% CL varies between $\pm 0.9^\circ$ to $\pm 1.8^\circ$, even allowing for maximal breaking between θ' and θ . It may be expected that the effect of penguin contributions in other decays, such as $B^0 \rightarrow J/\psi K_S^0$, should be limited to similar values, even if there is no strict flavor symmetry relating the mode to $B^0 \rightarrow J/\psi\rho^0$. Our limit is consistent with theoretical predictions [32].

We also set limits on the strong decay amplitude. Fig. 7 shows the 68% and 95% confidence levels contours for the penguin amplitude parameters of a' and θ' with a $-2\ln\mathcal{L}$ change of 2.3 and 6 units, for ndf equals two, including systematic uncertainties. They are obtained by converting the corresponding contours for $\alpha_{CP}^{J/\psi\rho}$ and $\Delta 2\beta_f$ using their relationship given in Eq. (5). The uncertainty on the angle $\gamma = (70.0^{+7.7}_{-9.0})^\circ$ only introduces about a 0.2% increase in the mean contour radius of a' versus θ' . The one-dimensional 68% confidence level intervals are found by changing $-2\ln\mathcal{L}$ by one unit, giving $a' < 0.12$ and $\theta' \in (190^\circ, 355^\circ)$, or $a' = 0.035^{+0.082}_{-0.035}$ and $\theta' = (285^{+69}_{-95})^\circ$.

The decay $B^0 \rightarrow J/\psi\pi^0$ proceeds through a similar diagram to that shown in Fig. 1, and thus the CP -violating parameters S and C should be similar to those we find in $B^0 \rightarrow J/\psi\rho^0$. These parameters are related to the parameter λ_f via the relationships

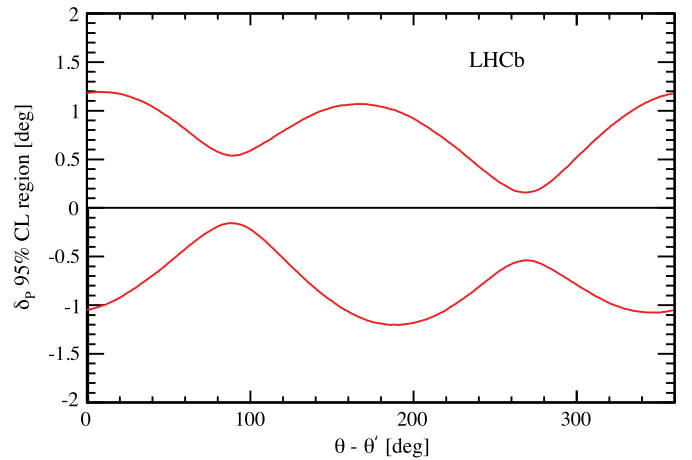


Fig. 6. The limit on the penguin induced phase change δ_P as a function of the difference in the penguin amplitude strong phases in $b \rightarrow c\bar{c}s$ and $b \rightarrow c\bar{c}d$ transitions $\theta - \theta'$, for $a = a'$.

$$S_f \equiv \frac{2\text{Im}(\lambda_f)}{1 + |\lambda_f|^2} = -2\eta_f \frac{|\lambda_f| \sin 2\beta_f^{\text{eff}}}{1 + |\lambda_f|^2},$$

$$\text{and } C_f \equiv \frac{1 - |\lambda_f|^2}{1 + |\lambda_f|^2}, \quad (14)$$

where we set the CP eigenvalue $\eta_f = 1$ to compare with the CP -even mode $B^0 \rightarrow J/\psi\pi^0$.

Using S_f and C_f as fit parameters, we obtain from Fit 1 $S_{J/\psi\rho} = -0.66^{+0.13+0.09}_{-0.12-0.03}$ and $C_{J/\psi\rho} = -0.063 \pm 0.056^{+0.019}_{-0.014}$, with a correlation of -0.01 . Table 8 shows the comparison of S_f and C_f

Table 8
Comparison of S_f and C_f between different measurements.

f	Experiment	S_f	C_f	Correlation
$\overline{B}^0 \rightarrow J/\psi \rho^0$	LHCb	$-0.66^{+0.13+0.09}_{-0.12-0.03}$	$-0.063 \pm 0.056^{+0.019}_{-0.014}$	-0.01 (stat)
$\overline{B}^0 \rightarrow J/\psi \pi^0$	Belle [33]	$-0.65 \pm 0.21 \pm 0.05$	$-0.08 \pm 0.16 \pm 0.05$	-0.10 (stat)
$\overline{B}^0 \rightarrow J/\psi \pi^0$	BaBar [34]	$-1.23 \pm 0.21 \pm 0.04$	$-0.20 \pm 0.19 \pm 0.03$	0.20 (stat)

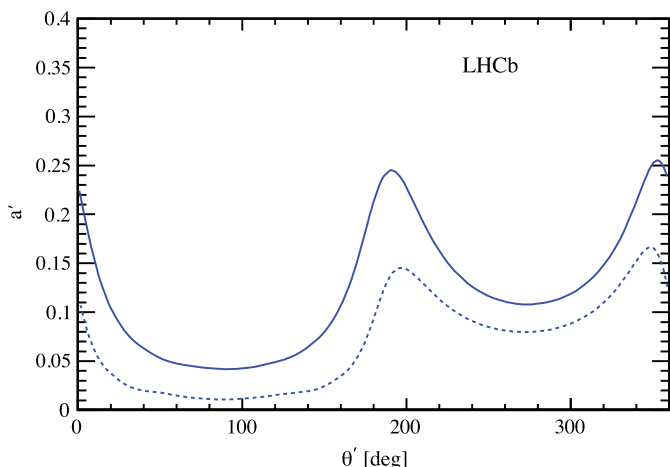


Fig. 7. Contours corresponding to 68% (dashed) and 95% (solid) confidence levels for ndf of two, respectively, for the penguin amplitude parameters a' and θ' .

from this measurement with that obtained from the Belle [33] and BaBar [34] Collaborations. Our measurements are in good agreement with the Belle results.

In conclusion, the measured value of the penguin contribution is $\delta_P = (0.05 \pm 0.56)^\circ = 0.9 \pm 9.8$ mrad. Taking the maximum breaking in phase and a range of breaking $0.5 < a/a' < 1.5$ the uncertainty on δ_P becomes ± 18 mrad. The measured value of ϕ_s currently has an uncertainty of about 35 mrad, and the value of 2β of 1.5° or 26 mrad [9]. Thus our limit is smaller than the current uncertainties, but will need to become more precise as the CP-phase measurements improve.

Acknowledgements

We express our gratitude to our colleagues in the CERN accelerator departments for the excellent performance of the LHC. We thank the technical and administrative staff at the LHCb institutes. We acknowledge support from CERN and from the national agencies: CAPES, CNPq, FAPERJ and FINEP (Brazil); NSFC (China); CNRS/IN2P3 (France); BMBF, DFG, HGF and MPG (Germany); SFI (Ireland); INFN (Italy); FOM and NWO (The Netherlands); MNiSW and NCN (Poland); MEN/IFA (Romania); MinES and FANO (Russia); MinEco (Spain); SNSF and SER (Switzerland); NASU (Ukraine); STFC (United Kingdom); NSF (USA). The Tier1 computing centres are supported by IN2P3 (France), KIT and BMBF (Germany), INFN (Italy), NWO and SURF (The Netherlands), PIC (Spain), GridPP (United Kingdom). We are indebted to the communities behind the multiple open source software packages on which we depend. We are also thankful for the computing resources and the access to software R&D tools provided by Yandex LLC (Russia). Individual groups or members have received support from EPLANET, Marie Skłodowska-Curie Actions and ERC (European Union), Conseil général de Haute-Savoie, Labex ENIGMASS and OCEVU, Région Auvergne (France), RFBR (Russia), XuntaGal and GENCAT (Spain), Royal Society and Royal Commission for the Exhibition of 1851 (United Kingdom).

References

- [1] S. Glashow, Partial symmetries of weak interactions, Nucl. Phys. 22 (1961) 579; S. Weinberg, A model of leptons, Phys. Rev. Lett. 19 (1967) 1264.
- [2] M. Kobayashi, T. Maskawa, CP violation in the renormalizable theory of weak interaction, Prog. Theor. Phys. 49 (1973) 652.
- [3] R. Fleischer, Recent theoretical developments in CP violation in the B system, Nucl. Instrum. Methods Phys. Res., Sect. A, Accel. Spectrom. Detect. Assoc. Equip. 446 (2000) 1, arXiv:hep-ph/9908340.
- [4] S. Faller, M. Jung, R. Fleischer, T. Mannel, The golden modes $B^0 \rightarrow J/\psi K_{S,L}$ in the era of precision flavor physics, Phys. Rev. D 79 (2009) 014030, arXiv:0809.0842; S. Faller, R. Fleischer, T. Mannel, Precision physics with $B_s^0 \rightarrow J/\psi \phi$ at the LHC: the quest for new physics, Phys. Rev. D 79 (2009) 014005, arXiv:0810.4248.
- [5] LHCb Collaboration, R. Aaij, et al., Measurement of the resonant and CP components in $\overline{B}^0 \rightarrow J/\psi \pi^+ \pi^-$ decays, Phys. Rev. D 90 (2014) 012003, arXiv:1404.5673.
- [6] LHCb Collaboration, R. Aaij, et al., Measurement of the CP-violating phase ϕ_s in $\overline{B}_s^0 \rightarrow J/\psi \pi^+ \pi^-$ decays, Phys. Lett. B 736 (2014) 186, arXiv:1405.4140.
- [7] A.S. Dighe, I. Dunietz, H.J. Lipkin, J.L. Rosner, Angular distributions and lifetime differences in $B_s^0 \rightarrow J/\psi \phi$ decays, Phys. Lett. B 369 (1996) 144, arXiv:hep-ph/9511363.
- [8] I.I. Bigi, A. Sanda, CP violation, Camb. Monogr. Part. Phys. Nucl. Phys. Cosmol. 9 (2000) 1.
- [9] Heavy Flavor Averaging Group, Y. Amhis, et al., Averages of b-hadron, c-hadron, and τ -lepton properties as of early 2012 and online update at <http://www.slac.stanford.edu/xorg/hfag>, arXiv:1207.1158, updated results and plots available at: <http://www.slac.stanford.edu/xorg/hfag/>.
- [10] Particle Data Group, K. Olive, et al., Review of particle physics, Chin. Phys. C 38 (2014) 090001.
- [11] R. Fleischer, Extracting CKM phases from angular distributions of $B_{d,s}$ decays into admixtures of CP eigenstates, Phys. Rev. D 60 (1999) 073008, arXiv:hep-ph/9903540.
- [12] LHCb Collaboration, A.A. Alves Jr., et al., The LHCb detector at the LHC, J. Instrum. 3 (2008) S08005.
- [13] R. Aaij, et al., Performance of the LHCb vertex locator, J. Instrum. 9 (2014) 090007, arXiv:1405.7808.
- [14] R. Arink, et al., Performance of the LHCb outer tracker, J. Instrum. 9 (2014) P01002, arXiv:1311.3893.
- [15] M. Adinolfi, et al., Performance of the LHCb RICH detector at the LHC, Eur. Phys. J. C 73 (2013) 2431, arXiv:1211.6759.
- [16] A.A. Alves Jr., et al., Performance of the LHCb muon system, J. Instrum. 8 (2013) P02022, arXiv:1211.1346.
- [17] R. Aaij, et al., The LHCb trigger and its performance in 2011, J. Instrum. 8 (2013) P04022, arXiv:1211.3055.
- [18] T. Sjöstrand, S. Mrenna, P. Skands, PYTHIA 6.4 physics and manual, J. High Energy Phys. 0605 (2006) 026, arXiv:hep-ph/0603175; T. Sjöstrand, S. Mrenna, P. Skands, A brief introduction to PYTHIA 8.1, Comput. Phys. Commun. 178 (2008) 852, arXiv:0710.3820.
- [19] I. Belyaev, et al., Handling of the generation of primary events in Gauss, the LHCb simulation framework, Nucl. Sci. Symp. Conf. Record (NSS/MIC) IEEE (2010) 1155.
- [20] D.J. Lange, The EvtGen particle decay simulation package, Nucl. Instrum. Methods Phys. Res., Sect. A, Accel. Spectrom. Detect. Assoc. Equip. 462 (2001) 152.
- [21] P. Golonka, Z. Was, PHOTOS Monte Carlo: a precision tool for QED corrections in Z and W decays, Eur. Phys. J. C 45 (2006) 97, arXiv:hep-ph/0506026.
- [22] Geant4 Collaboration, J. Allison, et al., Geant4 developments and applications, IEEE Trans. Nucl. Sci. 53 (2006) 270; Geant4 Collaboration, S. Agostinelli, et al., GEANT4: a simulation toolkit, Nucl. Instrum. Methods Phys. Res., Sect. A, Accel. Spectrom. Detect. Assoc. Equip. 506 (2003) 250.
- [23] M. Clemencic, et al., The LHCb simulation application, GAUSS: design, evolution and experience, J. Phys. Conf. Ser. 331 (2011) 032023.
- [24] L. Breiman, J.H. Friedman, R.A. Olshen, C.J. Stone, Classification and regression trees, Wadsworth International Group, Belmont, California, USA, 1984.

V. Syropoulos⁴², M. Szczekowski²⁸, P. Szczypka^{39,38}, T. Szumlak²⁷, S. T’Jampens⁴, M. Teklishyn⁷,
 G. Tellarini^{16,f}, F. Teubert³⁸, C. Thomas⁵⁵, E. Thomas³⁸, J. van Tilburg⁴¹, V. Tisserand⁴, M. Tobin³⁹,
 J. Todd⁵⁷, S. Tolks⁴², L. Tomassetti^{16,f}, D. Tonelli³⁸, S. Topp-Joergensen⁵⁵, N. Torr⁵⁵, E. Tournefier⁴,
 S. Tourneur³⁹, M.T. Tran³⁹, M. Tresch⁴⁰, A. Trisovic³⁸, A. Tsaregorodtsev⁶, P. Tsopelas⁴¹, N. Tuning⁴¹,
 M. Ubeda Garcia³⁸, A. Ukleja²⁸, A. Ustyuzhanin⁶⁴, U. Uwer¹¹, C. Vacca¹⁵, V. Vagnoni¹⁴, G. Valenti¹⁴,
 A. Vallier⁷, R. Vazquez Gomez¹⁸, P. Vazquez Regueiro³⁷, C. Vázquez Sierra³⁷, S. Vecchi¹⁶, J.J. Velthuis⁴⁶,
 M. Veltri^{17,h}, G. Veneziano³⁹, M. Vesterinen¹¹, J.V.V.B.Viana Barbosa³⁸, B. Viaud⁷, D. Vieira²,
 M. Vieites Diaz³⁷, X. Vilasis-Cardona^{36,p}, A. Vollhardt⁴⁰, D. Volyanskyy¹⁰, D. Voong⁴⁶, A. Vorobyev³⁰,
 V. Vorobyev³⁴, C. Voß⁶³, J.A. de Vries⁴¹, R. Waldi⁶³, C. Wallace⁴⁸, R. Wallace¹², J. Walsh²³,
 S. Wandernoth¹¹, J. Wang⁵⁹, D.R. Ward⁴⁷, N.K. Watson⁴⁵, D. Websdale⁵³, M. Whitehead⁴⁸,
 D. Wiedner¹¹, G. Wilkinson^{55,38}, M. Wilkinson⁵⁹, M.P. Williams⁴⁵, M. Williams⁵⁶, H.W. Wilschut⁶⁶,
 F.F. Wilson⁴⁹, J. Wimberley⁵⁸, J. Wishahi⁹, W. Wislicki²⁸, M. Witek²⁶, G. Wormser⁷, S.A. Wotton⁴⁷,
 S. Wright⁴⁷, K. Wyllie³⁸, Y. Xie⁶¹, Z. Xing⁵⁹, Z. Xu³⁹, Z. Yang³, X. Yuan³, O. Yushchenko³⁵,
 M. Zangoli¹⁴, M. Zavertyaev^{10,b}, L. Zhang³, W.C. Zhang¹², Y. Zhang³, A. Zhelezov¹¹, A. Zhokhov³¹,
 L. Zhong³

- ¹ Centro Brasileiro de Pesquisas Físicas (CBPF), Rio de Janeiro, Brazil
- ² Universidade Federal do Rio de Janeiro (UFRJ), Rio de Janeiro, Brazil
- ³ Center for High Energy Physics, Tsinghua University, Beijing, China
- ⁴ LAPP, Université de Savoie, CNRS/IN2P3, Annecy-Le-Vieux, France
- ⁵ Clermont Université, Université Blaise Pascal, CNRS/IN2P3, LPC, Clermont-Ferrand, France
- ⁶ CPPM, Aix-Marseille Université, CNRS/IN2P3, Marseille, France
- ⁷ LAL, Université Paris-Sud, CNRS/IN2P3, Orsay, France
- ⁸ LPNHE, Université Pierre et Marie Curie, Université Paris Diderot, CNRS/IN2P3, Paris, France
- ⁹ Fakultät Physik, Technische Universität Dortmund, Dortmund, Germany
- ¹⁰ Max-Planck-Institut für Kernphysik (MPIK), Heidelberg, Germany
- ¹¹ Physikalisches Institut, Ruprecht-Karls-Universität Heidelberg, Heidelberg, Germany
- ¹² School of Physics, University College Dublin, Dublin, Ireland
- ¹³ Sezione INFN di Bari, Bari, Italy
- ¹⁴ Sezione INFN di Bologna, Bologna, Italy
- ¹⁵ Sezione INFN di Cagliari, Cagliari, Italy
- ¹⁶ Sezione INFN di Ferrara, Ferrara, Italy
- ¹⁷ Sezione INFN di Firenze, Firenze, Italy
- ¹⁸ Laboratori Nazionali dell’INFN di Frascati, Frascati, Italy
- ¹⁹ Sezione INFN di Genova, Genova, Italy
- ²⁰ Sezione INFN di Milano Bicocca, Milano, Italy
- ²¹ Sezione INFN di Milano, Milano, Italy
- ²² Sezione INFN di Padova, Padova, Italy
- ²³ Sezione INFN di Pisa, Pisa, Italy
- ²⁴ Sezione INFN di Roma Tor Vergata, Roma, Italy
- ²⁵ Sezione INFN di Roma La Sapienza, Roma, Italy
- ²⁶ Henryk Niewodniczanski Institute of Nuclear Physics Polish Academy of Sciences, Kraków, Poland
- ²⁷ AGH – University of Science and Technology, Faculty of Physics and Applied Computer Science, Kraków, Poland
- ²⁸ National Center for Nuclear Research (NCBJ), Warsaw, Poland
- ²⁹ Horia Hulubei National Institute of Physics and Nuclear Engineering, Bucharest-Magurele, Romania
- ³⁰ Petersburg Nuclear Physics Institute (PNPI), Gatchina, Russia
- ³¹ Institute of Theoretical and Experimental Physics (ITEP), Moscow, Russia
- ³² Institute of Nuclear Physics, Moscow State University (SINP MSU), Moscow, Russia
- ³³ Institute for Nuclear Research of the Russian Academy of Sciences (INR RAN), Moscow, Russia
- ³⁴ Budker Institute of Nuclear Physics (SB RAS) and Novosibirsk State University, Novosibirsk, Russia
- ³⁵ Institute for High Energy Physics (IHEP), Protvino, Russia
- ³⁶ Universitat de Barcelona, Barcelona, Spain
- ³⁷ Universidad de Santiago de Compostela, Santiago de Compostela, Spain
- ³⁸ European Organization for Nuclear Research (CERN), Geneva, Switzerland
- ³⁹ Ecole Polytechnique Fédérale de Lausanne (EPFL), Lausanne, Switzerland
- ⁴⁰ Physik-Institut, Universität Zürich, Zürich, Switzerland
- ⁴¹ Nikhef National Institute for Subatomic Physics, Amsterdam, The Netherlands
- ⁴² Nikhef National Institute for Subatomic Physics and VU University Amsterdam, Amsterdam, The Netherlands
- ⁴³ NSC Kharkiv Institute of Physics and Technology (NSC KIPT), Kharkiv, Ukraine
- ⁴⁴ Institute for Nuclear Research of the National Academy of Sciences (KINR), Kyiv, Ukraine
- ⁴⁵ University of Birmingham, Birmingham, United Kingdom
- ⁴⁶ H.H. Wills Physics Laboratory, University of Bristol, Bristol, United Kingdom
- ⁴⁷ Cavendish Laboratory, University of Cambridge, Cambridge, United Kingdom
- ⁴⁸ Department of Physics, University of Warwick, Coventry, United Kingdom
- ⁴⁹ STFC Rutherford Appleton Laboratory, Didcot, United Kingdom
- ⁵⁰ School of Physics and Astronomy, University of Edinburgh, Edinburgh, United Kingdom
- ⁵¹ School of Physics and Astronomy, University of Glasgow, Glasgow, United Kingdom
- ⁵² Oliver Lodge Laboratory, University of Liverpool, Liverpool, United Kingdom
- ⁵³ Imperial College London, London, United Kingdom
- ⁵⁴ School of Physics and Astronomy, University of Manchester, Manchester, United Kingdom
- ⁵⁵ Department of Physics, University of Oxford, Oxford, United Kingdom
- ⁵⁶ Massachusetts Institute of Technology, Cambridge, MA, United States

- ⁵⁷ University of Cincinnati, Cincinnati, OH, United States
⁵⁸ University of Maryland, College Park, MD, United States
⁵⁹ Syracuse University, Syracuse, NY, United States
⁶⁰ Pontifícia Universidade Católica do Rio de Janeiro (PUC-Rio), Rio de Janeiro, Brazil ^w
⁶¹ Institute of Particle Physics, Central China Normal University, Wuhan, Hubei, China ^x
⁶² Departamento de Física, Universidad Nacional de Colombia, Bogotá, Colombia ^y
⁶³ Institut für Physik, Universität Rostock, Rostock, Germany ^z
⁶⁴ National Research Centre Kurchatov Institute, Moscow, Russia ^{aa}
⁶⁵ Instituto de Física Corpuscular (IFIC), Universitat de València – CSIC, Valencia, Spain ^{ab}
⁶⁶ Van Swinderen Institute, University of Groningen, Groningen, The Netherlands ^{ac}
⁶⁷ Celal Bayar University, Manisa, Turkey ^{ad}

* Corresponding author.

E-mail address: slstone@syr.edu (S. Stone).

- ^a Universidade Federal do Triângulo Mineiro (UFTM), Uberaba-MG, Brazil.
^b P.N. Lebedev Physical Institute, Russian Academy of Science (LPI RAS), Moscow, Russia.
^c Università di Bari, Bari, Italy.
^d Università di Bologna, Bologna, Italy.
^e Università di Cagliari, Cagliari, Italy.
^f Università di Ferrara, Ferrara, Italy.
^g Università di Firenze, Firenze, Italy.
^h Università di Urbino, Urbino, Italy.
ⁱ Università di Modena e Reggio Emilia, Modena, Italy.
^j Università di Genova, Genova, Italy.
^k Università di Milano Bicocca, Milano, Italy.
^l Università di Roma Tor Vergata, Roma, Italy.
^m Università di Roma La Sapienza, Roma, Italy.
ⁿ Università della Basilicata, Potenza, Italy.
^o AGH - University of Science and Technology, Faculty of Computer Science, Electronics and Telecommunications, Kraków, Poland.
^p LIFAELS, La Salle, Universitat Ramon Llull, Barcelona, Spain.
^q Hanoi University of Science, Hanoi, Viet Nam.
^r Università di Padova, Padova, Italy.
^s Università di Pisa, Pisa, Italy.
^t Scuola Normale Superiore, Pisa, Italy.
^u Università degli Studi di Milano, Milano, Italy.
^v Politecnico di Milano, Milano, Italy.
^w Associated to: Universidade Federal do Rio de Janeiro (UFRJ), Rio de Janeiro, Brazil.
^x Associated to: Center for High Energy Physics, Tsinghua University, Beijing, China.
^y Associated to: LPNHE, Université Pierre et Marie Curie, Université Paris Diderot, CNRS/IN2P3, Paris, France.
^z Associated to: Physikalisches Institut, Ruprecht-Karls-Universität Heidelberg, Heidelberg, Germany.
^{aa} Associated to: Institute of Theoretical and Experimental Physics (ITEP), Moscow, Russia.
^{ab} Associated to: Universitat de Barcelona, Barcelona, Spain.
^{ac} Associated to: Nikhef National Institute for Subatomic Physics, Amsterdam, The Netherlands.
^{ad} Associated to: European Organization for Nuclear Research (CERN), Geneva, Switzerland.